Ultrasonics Sonochemistry 21 (2014) 790–801

Contents lists available at ScienceDirect

Ultrasonics Sonochemistry

journal homepage: www.elsevier.com/locate/ultson

Ultrasonic assisted arsenate adsorption on solvothermally synthesized calcite modified by goethite, α-MnO_2 and goethite/α-MnO_2

Jasmina S. Markovski [a,*], Veljko Đokić [b], Milutin Milosavljević [b], Miodrag Mitrić [a], Aleksandra A. Perić-Grujić [b], Antonije E. Onjia [a], Aleksandar D. Marinković [b]

[a] Vinča Institute of Nuclear Sciences, University of Belgrade, PO Box 522, 11001 Belgrade, Serbia
[b] Faculty of Technology and Metallurgy, University of Belgrade, Karnegijeva 4, 11120 Belgrade, Serbia

ARTICLE INFO

Article history:
Received 21 June 2013
Received in revised form 27 September 2013
Accepted 8 October 2013
Available online 26 October 2013

Keywords:
Arsenate
Calcite
Goethite
α-MnO_2
Adsorption
Ultrasound

ABSTRACT

A highly porous calcium carbonate (calcite; sorbent **1**) was used as a support for modification with α-FeOOH (calcite/goethite; sorbent **2**), α-MnO_2 (calcite/α-MnO_2; sorbent **3**) and α-FeOOH/α-MnO_2 (calcite/goethite/α-MnO_2; sorbent **4**) in order to obtain a cheap hybrid materials for simple and effective arsenate removal from aqueous solutions. The adsorption ability of synthesized adsorbents was studied as a function of functionalization methods, pH, contact time, temperature and ultrasonic treatment. Comparison of the adsorptive effectiveness of synthesized adsorbents for arsenate removal, under ultrasound treatment and classical stirring method, has shown better performance of the former one reaching maximum adsorption capacities of 1.73, 21.00, 10.36 and 41.94 mg g^{-1}, for sorbents **1**–**4**, respectively. Visual MINTEQ equilibrium speciation modeling was used for prediction of pH and interfering ion influences on arsenate adsorption.

1. Introduction

Arsenic, a highly toxic metalloid, is recognized to be one of the world's greatest environmental hazards affecting to several hundred million people in more than 70 countries on six continents with the greatest influence on Bangladesh and India [1,2]. Arsenic occurs naturally in geological formations and as a result of geothermal and volcanic activity [3]. Generally, coal burning is consider to be major anthropogenic source of arsenic contamination among mining, fossil energy production, waste disposal and indiscriminate use of certain pesticides and wood preservatives [1,3,4].

In terms of arsenic toxicity based on epidemiological data from Taiwan, in 1993 the World Health Organization (WHO) reduced its guideline value from 50 to 10 μg/L as maximum concentration level of arsenic in drinking water [1,5]. Since arsenic toxicity to organisms depends on its chemical structure it is important to define form which could be inorganic (arsenite, arsenate, methylated arsenicals) and organic (arsenocholine, arsenobetaine, arseno-sugars, thioarsenates) [3,4]. Inorganic arsenicals are the most toxic forms and the effects of chronic exposure include skin lesions, disease of liver and kidney, cardio-vascular and peripheral vascular disease, neurological effect, diabetes and lung disease, while prolonged exposure leads to skin, bladder, liver and lungs cancer and thereby to death [1,3,6,7]. These data was the basis for the U.S. Environmental Protection Agency (EPA) classification of inorganic arsenic in Group A as a known human carcinogen [3].

Among available commercial techniques for arsenic removal such as coagulation and flocculation, adsorption and exchangers, membrane filtration, precipitation processes and alternative ozone, biological, electrochemical and solar techniques [8], adsorption takes special place as a simple, efficient and economic operation method offering flexibility in design and generating high-quality treated effluent [9,10]. As a result of geochemical transformation of arsenic in environment, considerable research has been devoted to study interaction of arsenate and calcite, and uses as adsorbent for water treatment [11]. Results of experimental studies suggested that fast arsenic adsorption was attributed to presence of Fe-oxides/oxyhydroxides rather than calcite itself [11].

Between the numerous adsorbents, nanosized metal oxides including: ferric [8,9,12], manganese, aluminium, titanium, magnesium, cerium, zirconium and alumina [9], possess various advantages such as fast kinetics, high capacity and specific affinity for heavy metal adsorption from aqueous system [9]. Several iron hydroxides/oxyhydroxides/oxides, natural or synthetic, are well known arsenic adsorbents [9,12]. The subject of numerous studies are goethite (α-FeOOH), hematite (α-Fe_2O_3), amorphous hydrous Fe oxides, maghemite (γ-Fe_2O_3), magnetite (Fe_3O_4) and iron/iron oxide (Fe@Fe_xO_y) [9]. Also, nanostuctured manganese(IV) oxide [13], alone or as iron-manganese binary oxide system [14,15], has been investigated in arsenate sorption studies where α-MnO_2 is the most commonly used polymorphic form. However, after all ben-

* Corresponding author. Tel.: +381 11 3303750.
E-mail address: jasmina.markovski@tmf.bg.ac.rs (J.S. Markovski).

1350-4177/$ - see front matter © 2013 Elsevier B.V. All rights reserved.
http://dx.doi.org/10.1016/j.ultsonch.2013.10.006

efits of nanostructured materials, the small diameter of metals nanoparticles demand impregnation into/onto porous support of large surface size to overcome activity loses due to agglomeration [9].

Many researchers have used ultrasonic treatment in the adsorption process of environment contaminant removal [16–18] due to its significant influence on adsorption which could be essentially manifested as increasing overall mass transfer in the pores [19–21]. Hamdaoiu and Naffrechoux reported that adsorption rate and adsorbent capacities, as well as intraparticle diffusion coefficient were remarkably improved under ultrasonic treatment [22]. The ultrasonic assisted enhancement of pollutant adsorption could be attributed to the high intensity processes generated during the violent collapse of cavitation bubbles. It was shown that sonication could produce not only high-speed micro-jets but also high-pressure shock waves and acoustic vortex microstreaming [18,23–26]. Acoustic microstreaming enhance the mass and heat transfer at interfacial films surrounding adsorbent surface. All of these effects contribute to effective pollutant adsorption by an enhancement of mass transfer through the bulk of solution, the boundary film at adsorbent surface and through the pores of the adsorbent particles [18].

Ultrasonic frequency cause cavitation extent, mass transport and concomitantly could produce detrimental effect to material integrity. If the frequency of applied ultrasound wave is above 16 kHz, transmitted irradiation through solution cause a series of compression and rarefaction waves resulting in the formation of microbubbles [27]. Due to microbubbles implosion, high pressures and temperatures are generated producing cavitation-strong hydrodynamic shear forces in the surroundings [28] which could result in the mechanical destruction, free radical formation and cause intensification of diffusion processes [29,30]. At very high frequencies, the compression/decompression cycle is too short to allow separation of solvent molecule to form a void, and cavitation is no longer obtained [31]. In a heterogenous system due to asymmetrical collapsing of the bubbles a high-speed jet of liquid near to a particle surface was created, it passes through the interior of the cavitation bubble and toward the solid surface, and could reach speeds of more than 100 ms^{-1} [32,33]. A scanning electron microscopy was used for the morphological characterization of the adsorbents surface before and after ultrasound treatment. Results showed no changes in the surface morphologies before and after sonication indicating no erosion.

In tune with above mentioned facts, this work describe ultrasonically assisted arsenate removal at varying pH, concentration, temperature and contact time. Aim of this research was to investigate the adsorption properties of high-surface-area porous calcite, and also its modification with goethite, α-MnO_2 and goethite/α-MnO_2 hybrid system. Starting material, highly porous calcite, and ones used for calcite modification, *i.e.* preparation of hybrid adsorbents **2**–**4**, are naturally abundant, inexpensive and effective adsorbents for arsenate removal. Chemical properties, high surface area and adsorption capacity of goethite [10] and manganese(IV) oxide, and even better properties and higher arsenate uptake of Fe–Mn binary oxides [15], were optimal alternatives for calcite modification. Additionally, for further interpretation of the adsorption equilibrium and understanding of adsorption mechanism, Visual MINTEQ [34] freeware program package was applied.

2. Matherials and methods

2.1. Materials

Arsenate working solutions were freshly prepared from $Na_2HAsO_4{}^*7H_2O$ (Sigma Aldrich) and deionized (DI) water (18 MΩ cm resistivity). Stock solution was preserved with 0.5% trace ultra-pure nitric acid (Fluka), and further solutions were diluted with deionized water to required metal ion concentration. All chemicals used in synthesis and in study of interfering ions: calcium oxide (CaO), poly(*N*-vinyl-2-pyrrolidone K90 (PVP), oleic acid (OA), ethanol (EtOH), iron(II) sulphate heptahydrate ($FeSO_4{}^*7H_2O$), sodium hydrogen carbonate ($NaHCO_3$), potassium permanganate ($KMnO_4$), manganese(II) sulphate monohydrate ($MnSO_4{}^*H_2O$), acetic acid (CH_3COOH), sodium dihydrogen phosphate (NaH_2PO_4), sodium sulphate (Na_2SO_4), silicic acid (H_4SiO_4), potassium nitrate (KNO_3), calcium(II) nitrate tetrahydrate $Ca(NO_3)_2{}^*4H_2O$ and magnesium(II) nitrate hexahydrate $MgNO_3{}^*6H_2O$ were obtained from Fluka.

2.2. Adsorbents preparation

General scheme of the applied synthesis methods and processes for sorbents **1**, **2**, **3** and **4** preparation are presented in Fig. 1, with following details on adsorbent synthesis:

Sorbent **1**, high-surface-area porous calcium carbonate, calcite polimorphic form, was prepared by solvothermal synthesis starting form morphologicaly irregular CaO powder as Ca source [35]. Well-defined morphologies, *i.e.* controled nucleation of crystallite, porosity of deposite, particles growth and alignment, of prepared adsorbents were achieved *via* proper selection of surfactant and porosity controll agent, system OA/PVP, as well as through solvo- and temperature-assisted processes. Solution of 14.8 g of PVP in 400 cm^3 oleic acid/ethanol mixture (v/v 1:1) was obtained under magnetic stirring. Then, 7.5 g of CaO was added to provide 1:0.625 M ratio of CaO/surfactant. The obtained solution was transferred to a stainless steel 500 cm^3 pressure reactor (Paar Instrument Company, Moline, USA), and subjected to solvothermal treatment at 200 °C for 6 h. Product was filtered, washed with DI water (100 cm^3), and dried in a dessicator for 48 h. Before calcination slow heating rate was applied, 1 °C/min, to promote larger porosity and compactness of grain, and after tretaed in air at 550 °C for 3 h. Before further modification, sorbent **1** was sonicated in a DI water for 1 h at 25 °C to remove any adsorbed material, vacuum filtered and wet used in next step of other sorbents synthesis.

Synthesis of sorbent **2**, calcite modified by goethite, was carried out in a following way: 1 g of sorbent **1**, 100 cm^3 of $FeSO_4{}^*7H_2O$ solution was subjected to mixing under N_2 for 30 min, and following by additon of 11 cm^3 of 1 mol dm^{-3} $NaHCO_3$ buffer solution. Variety of iron(II) concentration (0.5%, 1.0%, 1.5%, 2.0% and 2.5%) was used to perform synthesis of sorbent **2** in order to optimize adsorbent properties. Instead of nitrogen, air was used to provide oxygen containing atmoshere, and process was continued for 48 h under moderate mixing while suspension changed color from green–blue to ocherous as indication that oxidation process was completed [36]. Products was filtered, washed by DI water and dried in vacuum oven at 40 °C for 8 h.

Sorbent **3**, α-MnO_2 modified calcite composite material was prepared by *in situ* method as described by Than et al. [13] for modification of laterite. Sorbent **1**, 1.3 g, and $KMnO_4$, 0.22, 0.44 or 0.66 g, were dispersed in 30 cm^3 of DI water under magnetic stirring for 20 min at 60 °C. Solution prepared by mixing 0.858 g of $MnSO_4{}^*H_2O$ and 20 cm^3 of 1 M CH_3COOH at room temperature for 30 min was poured into dispersions of $CaCO_3$ modified with $KMnO_4$, and heated at 80 °C for 2 h. Products was cooled to room temperature, filtered, washed several time with DI water, and dried in a vacuum oven at 80 °C for 12 h.

Sorbent **4**, the hybrid material goethite/α-MnO_2 coated calcite, were prepared according to literature method [10]: 1.3 g of sorbent **1** was immersed in 65 cm^3 of different concentration: 0.05, 0.1, 0.5 and 1.0 mol dm^{-3} $FeSO_4{}^*7H_2O$ solution and subjected to mixing for 2 h to provide equilibration of the system. After filtration, the obtained material was redispersed in water under ultrasound treatment and added to $KMnO_4$ solution to provide equimolar

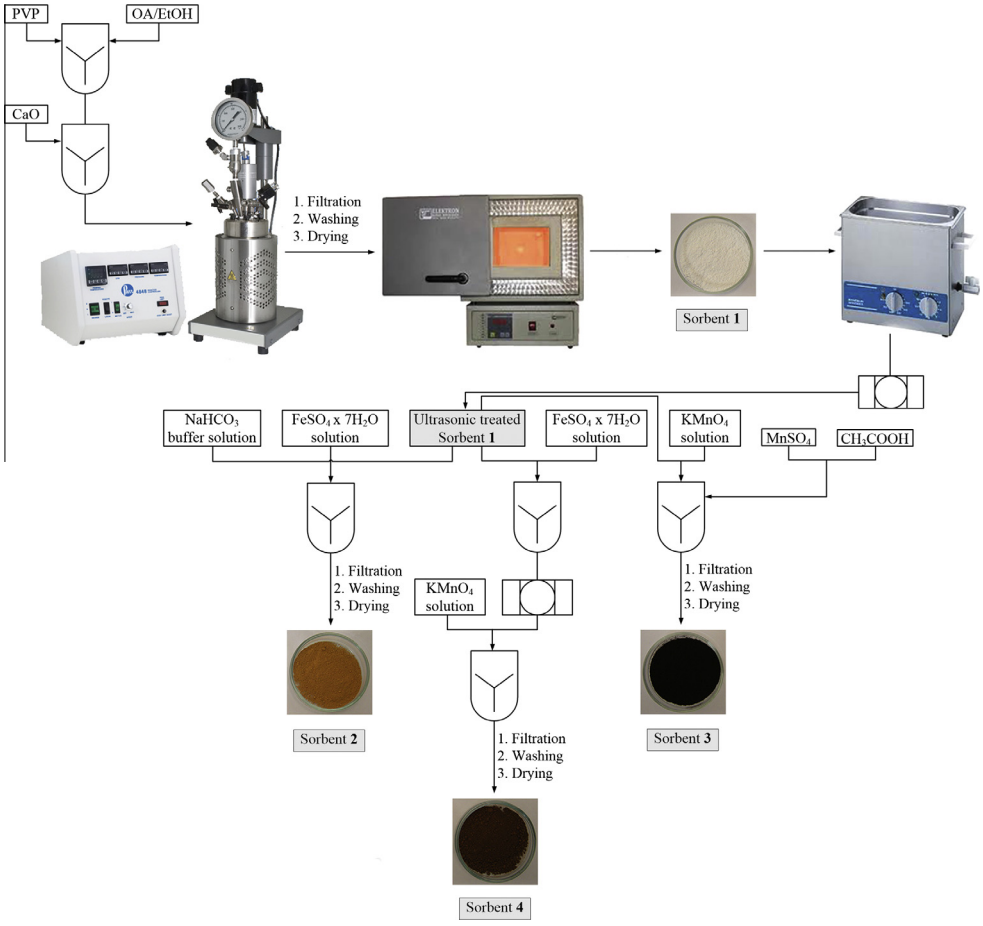

Fig. 1. General scheme of the applied synthesis methods and processes for sorbents preparation.

quantity of oxidant with respect to Fe(II) ions to perform ferrous-ferric oxidation. However, in contrast to previous work [10], the oxidation was performed at pH 7 to promote precipitation of α-MnO_2 forming goethite/α-MnO_2 hybrid adsorbent deposited on calcite support. After mixing for 2 h, dispersion was filtered, washed and isolated material was dried in a vacuum oven at 40 °C for 8 h.

2.3. Sorbent characterization

Specific surface area, pore volume and size distribution were measured by BET method on Micromeritics ASAP 2020MP surface area analyzer using nitrogen adsorption–desorption isotherm. X-ray diffraction (XRD) analysis were done on BRUKER D8 ADVANCE with Vario 1 focusing primary monochromator ($Cu_{k\alpha 1}$ radiation, $\lambda = 1.54059$ Å). Fourier-transform infrared spectra (FTIR) were collected on BOMEM (Hartmann & Braun) spectrometer, at room temperature, in 500–4000 cm^{-1} range with resolution of 4 cm^{-1} and sixteen scans. Samples for FTIR determination were prepared as KBr pellets (1.5 mg of sample and 200 mg of spectral grade KBr). The FTIR spectra was measured by a FTIR coupled with attenuated total reflection (ATR-FTIR), model Smart Orbit Nicolet 5700. Scanning electron microscope (FEG–SEM) was performed with field emission gun TESCAN MIRA3 electron microscope. A diameter of nanocomposites was determined using of MIRA TESCAN *in situ* measurement software. The Jeol 2100F transmission electron microscope (200 kV, Cs-corrected condenser, GIF Tridiem imagine filter) was used for imaging of the material structure.

The pH values at the point of zero charge (pH_{PZC}) of the samples, *i.e.* the pH above which the total surface of the samples is negatively charged, were determined according to the pH drift method [37]. The final pH (pH_{fin}), after equilibration (48 h), was measured and plotted against the initial pH (pH_{in}), and the pH_{PZC} was taken as cross section point of the line $pH_{fin} = pH_{in}$ [38].

2.4. Adsorption experiments

All adsorption experiments were conducted in a batch system under ultrasonic and conventional stirring treatment. Ultrasonic bath (Bandelin electronic, Berlin, Germany, power 120 W, frequency 35 kHz) was thermostated by circulating water through the jacket. All adsorption experiments, *i.e.* effect of time, pH and arsenate concentration were conducted at 25 ± 1 °C. Time-dependent arsenic adsorption was performed in a 100 mg dm^{-3} suspension, under ultrasonic treatment and stirring condition in a batch system, and sample was collected at 2, 3, 5, 10, 15, 20, 25, 30, 45, 60, 90 min and 2 h at pH 3.8 ± 0.1 and 25, 35 and 45 °C. Sufficient time of 45 min for quantitative arsenate removal was found for all sorbent materials. Influences of pH on arsenate adsorption was studied in a range of the initial pH values from 1 to 12, adjusted with 0.01 mol dm^{-3} NaOH and 0.1 mol dm^{-3} HNO_3, and measured by Mettler Toledo FE20/FG2 pH meter. The influence of temperature on arsenate adsorption (25, 35 and 45 °C) was carried out at pH 3.8 ± 0.1. The adsorbent isotherm and capacity were calculated according to the Eq. (1) with As(V) solution concentrations of 0.19, 0.81, 1.35, 1.90, 2.45, 3.21 and 4.1 mg dm^{-3} for sorbent **2**, and 0.19, 1.63, 2.53, 3.75, 4.97, 5.74 and 6.30 mg dm^{-3} for sorbent **4**, at pH 3.8 ± 0.1:

$$q = \frac{C_i - C_f}{m} V \quad (1)$$

where q is a adsorption capacity in mg g^{-1}, C_i and C_f are initial and final arsenic concentrations in mg dm^{-3}, respectively, V is the volume of solution in dm^3, and m is mass of adsorbent in g. Prior to analysis, the aqueous samples were filtered through 0.2 μm PTFE membrane filter, acidified with *conc*. nitric acid, stored in polyethylene containers and analyzed day after collection. Arsenic analysis was conducted by using inductively coupled plasma mass spectrometry (ICP-MS) by Agilent 7500ce ICP-MS system (Waldbronn, Germany). ICP-MS detection limit was 0.030 μg dm^{-3} and relative standard deviation (RSD) of all arsenic species investigated was between 1.3% and 5.1%.

2.5. Error functions

The best fitting model of adsorption isotherm was determined by the use of several mathematic error functions specified in work of Foo and Hameed [39]. The standard errors of kinetic and thermodynamic parameters were calculated by the use of commercial software (Microcal Origin 8.5) with a linear and/or non-linear least-square methods.

2.6. Modeling of the sorption processes

MINTEQ computer program was used for modeling of the adsorption processes, *i.e.* which includes two models: mathematical structure from MINEQL [40] and thermodynamic data base, temperature correction of equilibrium constants using either the Van't Hoff relationship and ionic strength correction using either the extended Debye–Hückel equation or the Davies equation from WATEQ3 [34]. Different surface complexation models and the database of Dzombak and Morel [41], utilized by Hering et al. [42], was incorporated in MINTEQ. The protonation/deprotonation properties of sorbent **2** was studied by glass electrode potentiometer, and corresponding constants were derived according to Diffuse Double Layer convention [43]. Protonation/deprotonation constants (log$K$) were given in Table S1, as well as arsenate intristic surface complexation constants and model parameters.

3. Results and discussion

3.1. Optimization of adsorbent preparation

In order to obtain high efficiency of arsenate removal and uniform/minimum quantity of coverage: goethite, α-MnO_2 and goethite/α-MnO_2 coating on calcite support, it was necessary to conduct optimization of synthesis procedure. Optimization goals, maxima of adsorption capacities and minimum of loaded oxides, were obtained for sorbent **2** (1.0% of $FeSO_4{}^*7H_2O$ solution), sorbent **3** (0.44 g of $KMnO_4$) and for sorbent **4** (65 cm^3 of 0.1 mol dm^{-3} $FeSO_4{}^*7H_2O$ solution and 1 g of $KMnO_4$). Except of experimental results, pH and goethite percentage loading influence on arsenate removal of sorbent **2** was modeled by MINTEQ program, and results are shown in Supplementary material.

3.2. Adsorbents characterization

Results of elemental composition (ICP-MS) and specific surface area, pore volume and mean pore diameter (BET analysis) for all adsorbents are presented in Tables S2 and S3, respectively.

The conditions of goethite, α-MnO_2 and goethite/α-MnO_2 deposition were crucial factor in synthesis methodologies which governs adsorption performance and the specific morphological properties of obtained sorbents. Additionally, fact that textural parameters of calcite was significantly lower than those of all synthesized sorbents provide an additional evidence that precipitation of goethite, α-MnO_2 and goethite/α-MnO_2 contributed to the increase of specific surface area, mesopore volume and diameter (Table S3). Generally, it is considered that adsorption capacity increases with a surface area and pore volume of adsorbents. Three different modifications of calcite, applied in this work, resulted in the highest surface area (264.32 m^2 g^{-1}), remarkable mesopore volume (0.532 cm^3 g^{-1}) and largest mesopore diameter (21.42 nm) contribute to maximum adsorption capacity of 41.94 mg g^{-1} for sorbent **4**. Such result was an indication that larger quantity of surface active sites could be avaliable for arsenate adsorption. Also, from the decrease of isoelectric point it could be concluded, according to literature finding [15], that specific adsorption, rather than a simple electrostatic interactions, is a mechanism has a larger contribution to overall sorption mechanism.

3.3. XRD analysis

To define phase and structure properties of synthesized sorbents **1**, **2**, **3** and **4**, the X-ray diffraction (XRD) analysis is applied and obtained patterns are shown on Fig. S1.

The XRD patterns of sorbent **1** show the typical crystalline phases of pure calcite (ICDD PDF2 No. 85-1108). Hybrid nature of calcite/goethite (sorbent **2**) is presented as new peaks at the angle 2θ of about 17.8°, 21.2°, 33.2°, 34.7° and 36.6° specific for goethite (ICDD PDF2 No. 81-0464). On diffraction pattern of sorbent **3** beside peaks of calcite the peaks of α-MnO_2 (ICDD PDF2 No. 44-0141) are present, which confirms that Mn introduced to calcite is α-MnO_2, but mainly in amorphous form. On the same diffraction pattern there can be noticed peaks of $CaSO_4$ (ICDD PDF2 No. 89-1458) which appears by transformation of $CaCO_3$ in presence of $MnSO_4{}^*H_2O$ in reaction of modification. In calcite/goethite/α-MnO_2 (sorbent **4**) presence of goethite (ICDD PDF2 No. 81-0464) and α-MnO_2 (ICDD PDF2 No. 44-0141) are evident. Beside their peaks there can be spotted $Ca(SO_4)(H_2O)_{0.5}$ (ICDD PDF2 No. 83-0439) and $FeSO_4(H_2O)_7$ (ICDD PDF2 No. 76-0657) peaks. For the same reason explained above $CaCO_3$ is replaced by $Ca(SO_4)(H_2O)_{0.5}$ and there is some amount of unreacted $FeSO_4(H_2O)_7$. Additionally, semi-quantitative XRD analysis showed 5.8% of goethite phase content in sorbent **2**, 25.6% of α-MnO_2 in sorbent **3**, 17.3% of goethite and 13.1% of α-MnO_2 in sorbent **4**.

3.4. Morphological characterization

Morphology and nanostructure in the nanocomposite material were studied by the FEG-SEM and TEM analysis (Figs. S2 and S3). Fig. S2 shows SEM images of sorbents **1**, **2**, **3** and **4** with magnification of 500 and 50, respectively.

The calcite appears to be granular structure with irregular shape, smooth surface and no sharp edges with the mean diameter of 200–500 nm. The goethite introduction to calcite does not affect significantly shape and size of basic structure, however, irregular sharp structure of 50–100 nm appeared on the material surface creating occasionally multilayer structure. α-MnO_2 entirely cover main structure of calcite with small 50 ± 9 nm sharp protuberances between which similar cavities occurs. Complete formed needle like uniform structure is on calcite/goethite-α-MnO_2. Needle size is about 200 ± 11 nm in length and 20 ± 4 nm in width with sharp cut peak but with no preferential direction. Additionally, TEM analysis was applied in order to evaluate morphologies of the obtained nanocomposites, *i.e.* the interaction of the goethite and the functional groups at the surface of the calcite (Fig. S3).

3.5. FTIR analysis

Analysis of the FTIR spectra of the investigated adsorbents is a useful method to obtain information about the presence of functional groups at adsorbent surface and interaction between surface functional groups and adsorbed arsenate oxyanion. FTIR analysis was performed to obtain qualitative estimations of the differences in the spectra of the adsorbent before and after adsorption. Such analysis is based on evaluation of the differences in the peak intensity, peak shifting and peak appearance or disappearance, as an indication of the types of adsorbate/-adsorbent interaction. Formation of surface complexes or any kind of electrostatic interactions resulted in bond strength changes, *i.e.* vibration frequencies of the group and thus changes in the wavelength values. Band shifts to lower or higher frequencies indicates bond weakening or strengthening, respectively. FTIR spectra of adsorbents **1**, **2**, **3** and **4**, before and after reaction with arsenate solution (4 mg dm^{-3}) are given in Fig. S4.

Spectrum of non-treated calcite (Fig. S4) show characteristic FTIR peaks at 713 cm^{-1}, 875 cm^{-1} and 1446 cm^{-1} in agreement with three active main bands at 714 cm^{-1} (ν_4 in plane band), 879 cm^{-1} (ν_2 out of plane band), 1432 cm^{-1} (ν_3 anti-symmetric stretching) and one inactive at 1097 cm^{-1} (ν_1 symmetric stretching) reported by Cifrulak [44]. Broad band observed at 1446 cm^{-1} is attribute to C–O stretching mode of carbonate, and as a result of different modification, peak is gradually weakened in spectra from sorbent **2** to **3**, and completely disappeared in spectrum of sorbent **4**. This result reflect high integrity of goethite/α-MnO_2 deposit and chemical compatibility with calcite surface functional groups. In spectra of sorbent **2** characteristic peaks are observed at 1126, 1040 and 976 cm^{-1} due primarily to the bending vibration of hydroxyl groups (Fe–OH) of iron(hydr)oxides vibration [14,15]. For sorbent **3**, the peak at 518 cm^{-1} is assigned to the Mn–O and Mn–O–Mn broad band vibrations at the low-frequency region [45]. The spectra of sorbent **4** shows complex structure peaks contribution indicating that not only physical interaction of two separate phases but also intensive chemical interaction significantly changes vibration modes which was found for individual phases.

Differences between bands structure in spectra of pure calcite, calcite/goethite, calcite/α-MnO_2 and calcite/goethite/α-MnO_2 before and after adsorptions of As(V) could be noticed from Fig. S4. Broad band at ≈3400 cm^{-1}, ascribed to OH and NH_2 stretching vibrations, asymmetric and symmetric, is not significantly affected by adsorbed anions. A gradual weakening of the Fe–OH bands (peaks at 1126, 1040 and 976) resulted in disappearance in spectra of calcite/goethite when the concentration of As(V) reached 4 mg dm^3. New band, corresponding to As–O stretching vibration of coordinated arsenic species, appeared at 800 cm^{-1}, which is close to literature finding (823 cm^{-1}) [14,15]. According to Myneni et al. [46] the force constant of the As–O–Fe bond increases with coordination number increase and decreases compared to uncomplexed As–O. The shorter bond distance results in a stronger force constant, *i.e.* higher infrared frequency. Consequently, the stretching vibration frequency of the uncomplexed/unprotonated As–O–Fe is located at higher position (866 cm^{-1}), while the frequency of the complexed As–O–Fe band is located at lower frequency (823 cm^{-1}). At higher surface coverage bidentate binuclear complex is a preferential type of binding [47], where two of four As–O bonds are complexed to iron atom, and the remaining two are present as unprotonated and/or protonated, depending on pH. FTIR spectra of sorbent **3**, before and after adsorption, is not useful for explanation of bond formation, but irrespectively to that disappearance of the most intensive bands at 518 cm^{-1} in calcite/α-MnO_2 spectra, and its weakening is a indication that Mn–O band contribute to arsenate complexation. Similar observation was found for sorbent **4**, and together with appearance of the peak at 778 cm^{-1} (spectra calcite/goethite/α-MnO_2/As) indicates that both component of hybride material are involved in a arsenate complexation.

3.6. Influence of pH on arsenate adsorption

The percentage of arsenate removal on sorbents **2** and **4** as a function of pH is presented in Fig. 2. Analogous pH-dependent study was performed for sorbents **1** and **3**. Results showed negligible capacity of sorbent **1** (1.73 mg g^{-1}) and only 50% capacity of sorbent **2** or 25% of sorbent **4** for sorbent **3**. Therefore sorbents **1** and **3** are not included in forthcoming discussion. Additionally, a two set of experiments were conducted to evaluate adsorption capacity of natural calcite based materials tufa (Temska, Pirot, Serbia) and $CaCO_3$ (grinded material used for water dispersive dyes, 5 μm). It was found that natural tufa contains a significant amount of iron (ICP, ≈9%), which is well-known high affinity sorbent for arsenic species. Results of adsorption studies showed that in both tufa and $CaCO_3$, a low adsorption capacity, 0.84 and 0.12 mg g^{-1}, respectively, were found. Literature data attributed the presence of Fe-oxides/oxyhydroxides to improved adsorption ability of natural calcite [11], and goethite showed significant stability in a wide pH range, as well as thermodynamic stability and resistivity to oxidative environment [36]. Results obtained in this work indicate that presence of iron, probably molecular forms of low adsorptive capability or availability at adsorbent surface, in tufa has low contribution on improvement of adsorbent performances. Except of this, tufa modification with goethite and goethite/α-MnO_2 provide higher adsorption capacities, *i.e.* 11.33 and 18.92 mg g^{-1}, respectively, than tufa itself. From that point of view solvothermal synthesis of calcite is a good method for preparation of structural and morphological material for further modification providing high capacity adsorbent (Tables 1 and 2).

It is evident that arsenate adsorption on both sorbents **2** and **4** decreases with pH increasing above 9. In a tested pH range (1–12) and in the case of ultrasonic treatment, the maxima for arsenate removal are obtained in pH range 3.8–8.1 after which steeply decrease, and strongly depend on interactions of arsenic species and pH dependent surface charges. Triprotic arsenic acid (H_3AsO_4) is present in molecular form at pH<2, and mainly as anionic species ($H_2AsO_4^-$, $HAsO_4^{2-}$) at higher pH, and, as weak acid, shows usually the most effective adsorption at pH near p*Ka* [10]. At a pH value lower than pH_{PZC}, the metal oxide surface could be protonated and positively charged adsorbent surface favors

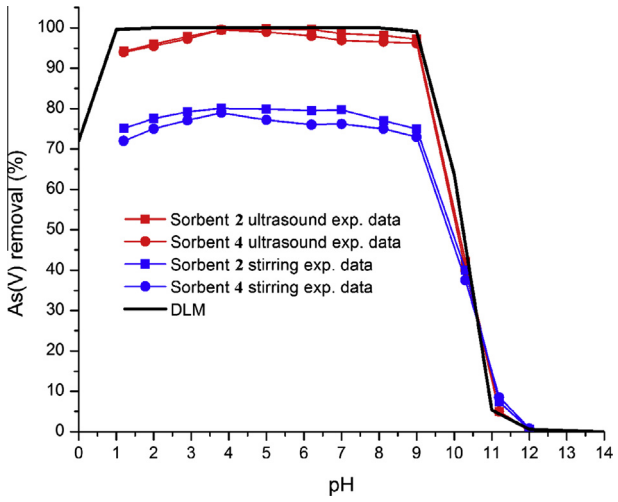

Fig. 2. Effect of pH and treatment applied on arsenate removal at 25 °C (t = 45 min, m/V = 100 mg dm^{-3}, $C_{As(V)}$ = 0.19 mg dm^{-3}).

Table 1
Adsorption isotherm parameters for arsenate removal on sorbent **2**.

Isotherm	Linear method			Non-linear method		
	25 °C	35 °C	45 °C	25 °C	35 °C	45 °C
Langmuir- type 1	$\frac{C_e}{q_e}=\frac{1}{bQ_0}+\frac{C_e}{Q_0}$			$q_e=\frac{Q_0 bC_e}{1+bC_e}$		
Q_o (mg g^{-1})	20.96	19.79	19.16	20.92	19.99	19.12
b (L mg^{-1})	79.73	4.77	2.85	108.55	4.61	2.78
R^2	0.9997	0.9996	0.9982	0.9954	0.9981	0.9977
Hill	$\log\left(\frac{q_e}{q_{sh}-q_e}\right)=n_h C_e-\log(K_D)$			$q_e=\frac{q_{sH}C_e^{n_H}}{K_D+C_e^{n_H}}$		
q_{sh} (mg dm^{-3})	21.23	19.63	20.59	20.71	19.55	20.59
n_H	0.82	1.03	0.89	1.00	1.00	0.87
K_D	0.03	0.19	0.48	0.005	0.19	0.48
R^2	0.9603	0.9978	0.9999	0.9971	0.9982	0.9993
Redlich–Peterson	$\ln\left(K_R\frac{C_e}{q_e}-1\right)=g\ln(C_e)+\ln(a_R)$			$q_e=\frac{K_R C_e}{1+a_R C_e^g}$		
a_R (mg^{-1})	98.03	3.89	4.76	99.98	4.56	3.83
g	1.00	0.90	0.97	1.00	1.00	0.91
K_R (dm^3 g^{-1})	2048.27	94.41	67.60	2053.62	92.05	66.40
R^2	0.9999	0.9999	0.9988	0.9914	0.9959	0.9945
Sips	$\beta_s\ln(C_e)=-\ln\left(\frac{K_s}{q_e}\right)+\ln(a_s)$			$q_e=\frac{K_s a_s C_e^{\beta_S}}{1+a_s C_e^{\beta_S}}$		
a_S (dm^3 mg^{-1})	160.24	6.39	3.23	209.89	5.35	2.09
β_S	0.26	0.50	0.52	1.00	1.00	0.87
K_S (dm^3 g^{-1})	3911.40	104.00	43.00	4346.05	104.64	42.96
R^2	0.7305	0.9168	0.9518	0.9971	0.9982	0.9993
Khan	–*			$q_e=\frac{q_s b_K C_e}{(1+b_K C_e)^{aK}}$		
q_s (mg g^{-1})				22.81	22.74	13.78
a_K				1.00	1.00	0.88
b_K				91.92	3.80	4.51
R^2				0.9964	0.9984	0.9997
Jovanovic–Freundlich	$\ln\left(-\ln\left(1-\frac{q_e}{q_m}\right)\right)=n\ln K_{JF}+n\ln C_e$			$q_e=q_m(1-\exp(-(K_{JF}C_e)^n))$		
q_m (mg g^{-1})	21.00	18.10	17.72	20.44	17.98	17.64
n	0.51	0.82	0.76	0.79	0.80	0.72
K_{JF} (dm^3 g^{-1})	29.66	3.21	1.82	65.28	3.39	1.88
R^2	0.9153	0.9981	0.9966	0.9969	0.9965	0.9970

* There is no linear model for Khan equation.

Table 2
Adsorption isotherm parameters for arsenate removal on sorbent **4**.

Isotherm	Linear method			Non-linear method		
	25 °C	35 °C	45 °C	25 °C	35 °C	45 °C
Langmuir-type 1	$\frac{C_e}{q_e}=\frac{1}{bQ_0}+\frac{C_e}{Q_0}$			$q_e=\frac{Q_0 bC_e}{1+bC_e}$		
Q_o (mg g^{-1})	42.29	40.78	37.52	41.81	41.74	41.52
b (L mg^{-1})	54.55	6.18	2.29	66.68	4.73	1.50
R^2	0.9999	0.9943	0.9618	0.9942	0.9940	0.9884
Jovanovic	$\ln\left(-\ln\left(1-\frac{q_e}{q_m}\right)\right)=\ln K_J+\ln C_e$			$q_e=q_m(1-\exp(-K_J C_e))$		
q_m (mg g^{-1})	41.95	41.71	41.53	40.34	36.86	33.05
K_J (dm^3 g^{-1})	5.65	1.64	1.15	49.78	3.82	1.52
R^2	0.9521	0.9947	0.9795	0.9792	0.9815	0.9928
Khan	–*			$q_e=\frac{q_s b_K C_e}{(1+b_K C_e)^{aK}}$		
q_s (mg g^{-1})				37.66	37.53	37.46
a_K				0.98	0.96	0.95
b_K				80.81	5.57	1.71
R^2				0.9950	0.9941	0.9847

* There is no linear model for Khan equation.

adsorption, *i.e.* electrostatic attraction, of negatively charged arsenate ions ($H_2AsO_4^-, HAsO_4^{2-}$).

Analogous experiments were performed using a glass reactor (conventional method; the same reaction geometry and adsorption conditions) and variable magnetic stirrer speed of 150–500 rpm. Noticeably, it was found that two adsorption methods applied, classical stirring and ultrasound treatment, produced significantly different results, *i.e.* adsorption capacity is reduced about 20% in the case of former. Ultrasound treatment is a effective method very often used for intensification and improvement of successfulness of adsorption processes [10,17,18–23]. Ultrasonic waves produce microscopic bubbles in the liquid which collapse creating shock waves, which are highly effective in increasing the material wetting and help in efficient conducting mass transfer controlled processes. These effects, associated with hydrodynamic phenomenon due to cavitation, are responsible for better adsorption

effectiveness under ultrasound assisted experiments. In accordance with that all forthcoming results, except kinetic study, are related to ultrasonically assisted arsenate adsorption on sorbents **1**–**4**.

Experimental results of pH influence on arsenate removal were modeled by using MINTEQ programme, and results presented in Fig. S5 show that the best fitting was obtained with diffuse layer model (DLM) for sorbent **2**. The DLM model, proposed by Stumm et al., and developed by Dzombak and Morel, was based on assumptions that surface is presented as two planes of charges with dominance of inner-sphere complexes, and without formation of surface complexes with ions in the background electrolyte [48]. Using input parameters given in Table S1 and modeling of the experimental data, high level of accordance of experimental data and theoretical results was obtained.

Studies on the influence of co-existing ions, as potential interferences to arsenic removal [49], were performed by modeling arsenate removal in the presence of phosphate, sulphate, silica, ionic strength, calcium and magnesium. Theoretical results were in accordance with experimental data and competing ions showed low effect on arsenate adsorption. Most of investigated anions had no significant influences on As(V) removal, while phosphate caused the greatest adsorption decrease. On the contrary, the presence of Ca^{2+} has no influences and Mg^{2+} slightly enhances the adsorption of As(V).

Phosphate has strong affinity for goethite, and due to similar chemical properties is considered to be major competitor with respect to arsenate [50]. At concentration higher than 5 mg dm^{-3} phosphate causes significant reduction of adsorption (Fig. S7). Results of sulphate, silica and ionic strength, interference studies showed absence or just a slight deterioration effect on the adsorption of As(V) (Figs. S8-S10). Low ionic strength influence on arsenate adsorption (Fig. S10), is a feature indicative for an inner-sphere adsorption mechanism [51,52]. Ca and Mg cations have no effect at lower concentration, but at higher (>10 mg dm^{-3}) Mg supports arsenate adsorption processes (Fig. S12). The used concentrations of competing anions are higher than arsenic concentration, indicating that adsorbents are able to remove arsenic species even in the presence of significant concentrations of competing anions. Presented results are in accordance with literature results related to arsenate adsorption on goethite [10] and Fe–Mn binary system [15].

The pH change during adsorption is an indication that protonation/deprotonation reactions of surface functional groups and adsorption of arsenic species are operative processes. pH_{fin}/pH_{in} dependence (Fig. S13) indicates that complex adsorption processes are operative and their contribution to pH change is different at appropriate pH_{in}. Differences in pH_{fin}/pH_{in} are almost constant low values up to pH 8, and they show similarity to constant percent of arsenate removal (Fig. 2). At $pH_{in} < pH_{PZC}$ high removal capabilities of sorbents **2** and **4** are mostly of electrostatic nature and ligand exchange phenomenon, *i.e.* formation of inner-sphere surface complexes. When $pH_{in} > pH_{PZC}$, increases of adsorbent surface group ionization and negatively charged divalent As(V) anion concentration, due to pH-dependent arsenic speciation [10], cause repulsion of negatively charged adsorbate surface groups/adsorbent pairs at boundary layer of the solid interface.

3.7. Adsorption isotherms

The two, three and multilayer physisorption isotherm models were applied in order to study the adsorption mechanism and to compute various adsorption parameters: Langmuir, Freundlich, Dubinin–Radushkevich, Tempkin, Flory–Huggins, Hill, Redlich–Peterson, Sips, Toth, Koble–Corrigan (K–C), Khan, Radke–Prausnitz, Brunauer–Emmett–Teller (BET) [39], Jovanovic and Jovanovic–Freundlich (J–F) [53].

Isotherm parameters of best fitting experimental data, based on highest correlation coefficient, obtained by linear and non-linear regression method are listed in Tables 1 and 2.

The Khan model fits well with the adsorption data for sorbent **2** and the Jovanovic model for sorbent **4**. Therefore, the Khan model better describes the adsorption behavior of sorbent **2**, and considering mathematically, according to a_k values calculated from experimental results obtained at 25 and 35 °C (Table 1), strive to Langmuir model. The maximum adsorption capacities, determined by using the Khan model, are higher than values obtained by Langmuir model while the order of the equilibrium constant b_k is similar to parameter b obtained from Langmuir isotherm at 25 °C. Jovanovic isotherm is a two parameter model based on Langmuir model which takes into account multilayer adsorption on homogenous surface, where q_m presents monolayer saturation and K_J is numerical coefficient. Jovanovic model describes adequately arsenate adsorption on sorbent **4**, and gave somewhat lower q_m value than Q_o obtained according to Langmuir model at 25 °C (Table 2). The linear and non-linear correlation coefficients for the Khan and Jovanovic models are similar, and for both sorbents, adsorption capacity decreases with an increase of temperature. The Langmuir adsorption model [54] was used for determination of adsorption capacity and K_L coefficient for thermodynamic parameters calculation. The maximum arsenate adsorption capacities obtained by Langmuir were 20.92 mg g^{-1} for sorbent **2** and 41.81 mg g^{-1} for sorbent **4**. The highest uptake of As(V) by the binary hybrid sorbent **4** may be due to its higher surface area (264.32 m^2 g^{-1}), mesopore volume (0.532 cm^3 g^{-1}) and mesopore diameter (21.42 nm) than those of other adsorbents. Additionally, hybrid sorbent include balanced (synergetic) characteristics of both goethite and α-MnO_2 components.

In order to evaluate the quality of fitting experimental data, the validation of different adsorption isotherms were accomplished using different error functions including also the correlation coefficient R^2. Using nonlinear regression instead of linear incorporates the minimization or maximization of error distribution between the experimental data and the predicted isotherms based on its convergence criteria. The data analysis was accomplished using Marquardt's percent standard deviation (MPSD); hybrid fractional error function (HYBRID); average relative error (ARE); average relative standard error (ARS); sum squares error (ERRSQ/SSE); standard deviation of relative errors (s_{RE}) and nonlinear chi-square test (χ^2) (Table 3) [39].

In addition, based on the use of eight mathematical error functions, the most suitable model is choosen (underlined values; Table 3). However, differences between linear and non-linear regression analysis should be noted: for linear analysis the highest value of R^2 is the most adequate error estimation tool, while in non-linear, the MPSD, HYBRID, ERRSQ/SSD are more appropriate, but for three-parameter model error function which takes into account different numbers of the model parameter (MPSD and HYBRID) are more important [55].

Graphical presentation of best fitting model obtained by nonlinear regression analysis, using Khan model for sorbent **2** and Jovanovic model for sorbent **4**, evaluated by appropriate mathematical errors, are shown in Figs. 3 and 4.

3.8. Adsorption kinetics

Arsenate removal at pH 3.8 was investigated by arsenate adsorption on sorbents **2** and **4** as a function of contact time. Results showed that the adsorption was fast process and 45 min was enough time to achieve quantitative removal of arsenate with sorbents **2** and **4**.

Table 3
Isotherm error deviation related to arsenate sorption using commonly used functions.

Error function	R^2	χ^2	MPSD	HYBRID	ARE	ARS	ERRSQ	s_{RE}
Linear approach for sorbent ***2***								
Langmuir	0.9997	0.5793	12.196	11.585	8.0826	0.1113	7.1544	8.1057
Hill	0.9603	0.6021	17.944	12.042	8.8179	0.1638	6.2656	9.2717
R-P	0.9999	0.0534	2.6944	1.3353	1.6897	0.0220	1.0010	1.7875
Sips	0.7305	293.90	587.21	7347.5	217.15	4.7945	912.60	244.73
J–F	0.9153	2.4121	38.908	60.303	18.190	0.3177	24.619	18.950
Non-linear approach for sorbent ***2***								
Langmuir	0.9954	0.0895	5.1323	1.7909	3.2807	0.0468	1.2402	3.6072
Hill	0.9971	0.0924	8.5122	1.8483	3.9112	0.0777	0.6379	4.1930
R-P	0.9954	0.0897	5.7539	2.2432	3.2856	0.0470	1.2401	3.6168
Sips	0.9971	0.0929	9.5579	2.3229	3.8975	0.0780	0.6395	4.1661
Khan	0.9964	0.0425	2.6198	1.0619	1.8204	0.0214	0.7920	1.9995
J–F	0.9943	0.0962	9.6327	2.4040	4.0219	0.0786	0.6837	4.3872
BET	0.9969	0.0911	5.8225	2.2767	3.3007	0.0475	1.2524	3.6310
Linear approach for sorbent ***4***								
Langmuir	0.9999	108.08	91.673	2081.7	76.364	0.8368	3493.0	60.952
Jovanovic	0.9521	7.8136	66.136	195.34	40.770	0.5400	148.10	40.059
Non-linear approach for sorbent ***4***								
Langmuir	0.9942	198.49	116.45	3969.8	98.421	1.0631	7210.8	76.757
Jovanovic	0.9792	0.6836	6.2294	13.671	4.0923	0.0569	25.177	4.8569
Khan	0.9950	0.5799	24.162	14.498	9.0501	0.1973	4.8558	9.9429

In order to investigate the kinetics of adsorption of As, different kinetic models (pseudo-first order or Lagergren model, pseudo-second order or Ho–McKay model, Roginsky–Zeldovich-Elovich equation and second-order rate equation), and adsorption diffusion models (liquid film linear driving force rate equation, liquid film diffusion mass transfer rate equation, homogeneous solid diffusion model, parabolic or Weber–Morris model, Dunwald–Wagner model and double exponential model) were used [56]. Non-linear regression of experimental data showed that the best fitting with intra-particle (Weber–Morris) model and the pseudo-second-order kinetic model, reported to be the most appropriate to describe chemisorption (Tables 4 and 5, Figs. 5 and 6).

Non-linear least-squares methods analysis of pseudo-second-order Eq. (2) and intra-particle (Weber–Morris) diffusion kinetic models Eq. (3) [57] showed the best regression coefficient for both sorbents.

$$\frac{t}{q_t} = \frac{1}{2K'q_e^2} + \frac{1}{q_e}t \tag{2}$$

$$q_t = k_p t^{0.5} + C. \tag{3}$$

The adsorption capacities at equilibrium and at time t (min) are defined by q_e and q_t (mg g^{-1}) respectively, K' is the pseudo-second-order rate constant of adsorption, k_p (mg g^{-1} min$^{-0.5}$) is the intraparticle diffusion rate constant, and C is the intercept of the line (mg g^{-1}) which is proportional to the boundary layer thickness.

The obtained kinetic parameters for arsenate adsorption, presented in Tables 4 and 5, indicate good sorbent affinity with respect to arsenate ion and fast adsorption process for both sorbent materials. The increased rate of adsorbate transport under ultrasonic treatment (Table 4) could be ascribed to high frequency fluid fluctuation, *i.e.* turbulent flow of the medium, which is a consequence of violent collapse of cavitation bubbles. Asymmetric collapse of the bubbles, due to system heterogeneity, produce micro-jet with high velocity enhancing mass and heat transfer through stationary film (interfacial film) surrounding adsorbent and also within the pores. Except of the formation of high-speed micro-jet, sonication could produce high-pressure shock wave and acoustic vortex microstreaming [18–26]. Due to this fact energetic barrier, *i.e.* activation energy, of the adsorption process is lower for ultrasonically assisted adsorption, 12.6 kJ mol^{-1}, vs. classical stirring method, 21.5 kJ mol^{-1} (Supplementary material). Higher rate of arsenate transport, under magnetic stirring, was provided by increasing mixing rate, from 150 to 500 rpm, but still significantly lower pseudo-second order rate constants were obtained (Table 4). Increased mixing rate cause turbulent flow and reduction of the thickness of the boundary layer or improve the diffusion coefficient in the bulk and in the film, resulting in enhancement of the mass transfer rate.

Due to heterogeneity of the system different mass transfer processes at different step could be significant contributing factor to the control of overall process. However, to predict the actual rate-controlling step involved in the adsorption process of As(V), the intraparticle Weber–Morris diffusion model was applied. The intra-particle diffusion model vs. the pseudo-second-order equation as a generalized, one rate-controlling step removal process, provides a more comprehensive insight into adsorption mechanism which is usually consisted of a series of distinct steps [58]. Generally, adsorption diffusion model is a process which consists of three consecutive steps where the first one presents diffusion across the liquid film to the adsorbent exterior surface, called external diffusion or film diffusion, the second is transport of adsorbate in the pores and/or along the pore walls, called internal or intra-particle diffusion, and last, third step is adsorption and desorption between adsorbate and active sites, *i.e.* mass action [56]. Results of applied Weber–Morris model are presented in Fig. 6. For both adsorbent materials, a plotted q_t vs. $t^{0.5}$ is a straight multi-linear curve which does not pass through the origin suggesting that the overall adsorption may be controlled by two or more steps. Therefore, first linear part demonstrates external mass transfer related not only to instantaneous adsorbate bonding at the most readily available adsorbing sites but also could be due to the contribution of adsorption at mesopore surface. This feature is highly dependable on specific surface area which is 255.22 and 264.32 m^2 g^{-1} for sorbents **2** and **4** respectively, and similar adsorption rate could be expected in the first adsorption step. In contrast to the similarity of specific surface area of sorbent **2** and **4**, large differences in mesopore volume (0.146 vs. 0.532) and mesopore diameter (2.90 vs. 21.42) (Table S3), respectively, could be an additional factor which contributes to differences in k_{p1} and k_{p2} values (Table 5). The second part is a process of gradual attainment of equilibrium which includes intra-particle diffusion

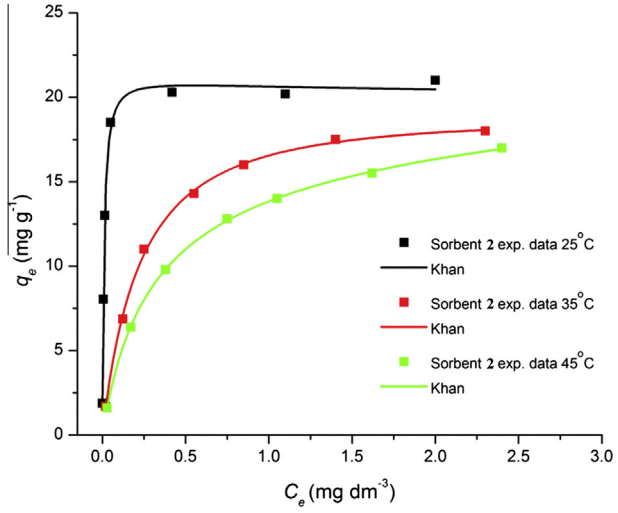

Fig. 3. Adsorption isotherms of arsenate onto sorbent **2** at 25, 35 and 45 °C (m/V = 100 mg dm^{-3}, $C_{As(V)}$ = 0.19, 0.81, 1.35, 1.90, 2.45, 3.21 and 4.10 mg dm^{-3}, pH = 3.8).

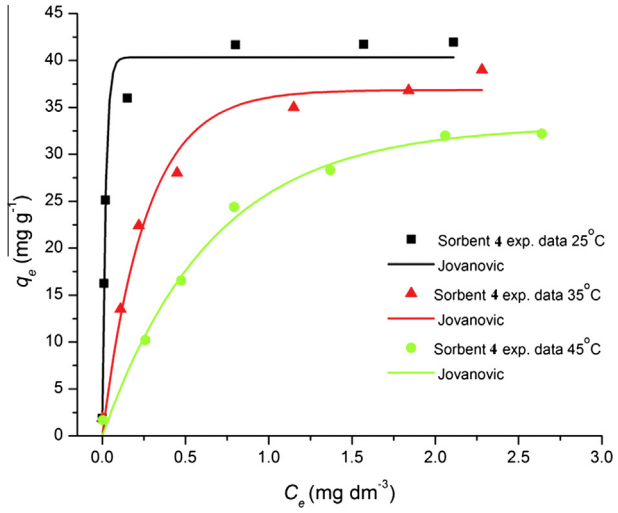

Fig. 4. Adsorption isotherms of arsenate onto sorbent **4** at 25, 35 and 45 °C (m/V = 100 mg dm^{-3}, $C_{As(V)}$ = 0.19, 1.63, 2.53, 3.75, 4.97, 5.74 and 6.30 mg dm^{-3}, pH = 3.8).

Table 4
Kinetic parameters of the pseudo-second-order equation for arsenate adsorption under ultrasonic treatment and classical magnetic mixing at 25 °C.

Sorbent		Ultrasound treatment		
		q_e (mg g^{-1})	K' (g mg^{-1} min^{-1})	R^2
2		2.040	0.088	0.989
4		2.053	0.141	0.984
	Mixing rate (rpm)			
2	150	1.466	0.018	0.989
	300	1.547	0.028	0.992
	500	1.723	0.041	0.991
4	150	1.756	0.088	0.988
	300	1.884	0.097	0.987
	500	1.987	0.103	0.995

as an intermediate mechanism, *i.e.* saturation of adsorptive sites in macro pores and increases of the process operative in micro pores. While in the course of final stage, *i.e.* third step, slow transport of arsenic species inside adsorbent micro pores dominate and attainment of adsorption–desorption equilibrium denote overall saturation of available adsorptive sites [59]. On the basis of intra-particle diffusion constant rate values (Table 5) it could be concluded that intra-particle diffusion is rate controlling step, largely prevailing over fast external mass transfer, and comparison between sorbents **2** and **4** showed larger intra-particle diffusion constant, *i.e.* lower k_{p2} and k_{p3} values for former, in tune with higher value of textural parameters of later one (Table S3).

3.9. Thermodynamic study

The Gibbs free energy (ΔG^o), enthalpy (ΔH^o) and entropy (ΔS^o) of adsorption were calculated using the Van't Hoff thermodynamic equations:

$$\Delta G^\circ = -RT\ln(b) \tag{4}$$

$$\ln(b) = \Delta S^\circ/R - \Delta H^\circ/(RT), \tag{5}$$

where T is the absolute temperature in K and R is the universal gas constant (8.314 J mol^{-1} K^{-1}). ΔH^o and ΔS^o can be obtained from the slope and intercept of $\ln(b)$ vs. $1/T$ plot, assuming the sorption kinetics to be under steady-state conditions. The calculated thermodynamic values (Table 6) give some information concerning the adsorption mechanism operative in investigated system.

The negative values of Gibbs free energy changes and positive standard entropy changes at all temperatures indicate that arsenate adsorption on both sorbent matherials is a spontaneous process. Sorbent **2** has the higher ΔG^o values compared with sorbent **4**, decreases with temperature indicating that spontaneity of adsorption increases at lower temperature. It is known that different contribution of physisorption and chemisorption was defined based on free energy change [60], and according to such classification arsenate sorption on studied adsorbents could be observed as contribution of both physisorption and chemisorption processes. The changes in entropy values were positive, indicating the increase in randomness due to adsorption of arsenate from the aqueous solution to the adsorbent. The negative values of ΔH^o show that arsenate adsorption on sorbents **2** and **4** are exothermic processes with more preferable adsorption at lower temperature. In summary, the enthalpy and free energy values were positive, which means that adsorption was more spontaneous at lower temperature, and entropy changes indicate that adsorption process on studied adsorbents was an entropy-driven process.

3.10. Desorption and reusability study

Desorption experiments were performed using sorbents **2** and **4**. Sodium hydroxide and strong acids are most commonly used to elute arsenate, and selection of eluent depends on the arsenic adsorption mechanism and nature of sorbent [61]. It was expected that OH^- ions should be strong anion which compete for the same adsorption sites occupied with arsenate ion. The most efficient desorption system was found to be NaOH/NaCl (0.5/0.5; mol dm^{-3}) for both sorbents. Desorption was enhanced at high pH values because arsenate ions were deprotonated and easily exchanged with hydroxyl ions. Irreversibly bonded arsenate was negligible, 92% and 98% for sorbents **2** and **4**, respectively, in a regeneration process of first cycle. Regenerability was achieved without significant influence on adsorptive performance in subsequent adsorption cycle. Throughout five consecutive cycles, desorption efficiency was decreased to 86% and 91% for sorbents **2** and **4**, respectively. Except of this, low extent of the leaching of iron and manganese species was found when presented methodology was applied. Ultrasound frequency influences the growth cycle of cavitation bubbles: at higher frequency cycles are shorter and exert less violent collapses and *vice versa*, at lower frequency [18–26]. Threshold intensity was not exceeded, meaning that under applied

Table 5
Kinetic parameters of the Weber–Morris intraparticular model for arsenate adsorption.

Sorbent	k_{p1} (mg g^{-1} min$^{-0.5}$)	R^2	C_1 (mg g^{-1})	k_{p2} (mg g^{-1} min$^{-0.5}$)	R^2	k_{p3} (mg g^{-1} min$^{-0.5}$)	R^2
2	0.313	0.994	0.217	0.118	0.889	0.011	0.940
4	0.466	0.944	0.116	0.161	0.908	0.013	0.888

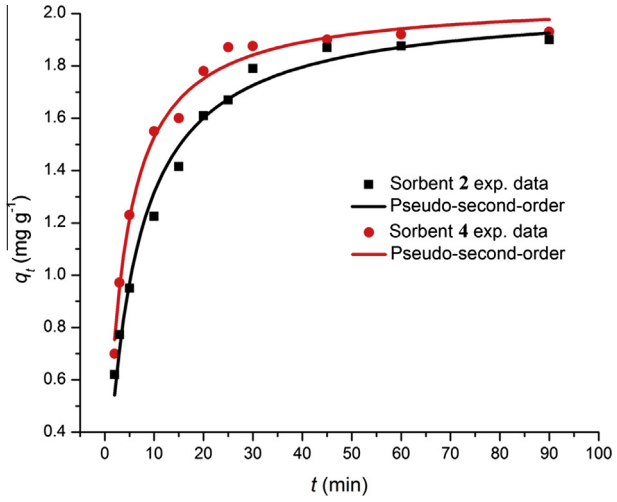

Fig. 5. Plot of pseudo-second order model for arsenate adsorption onto sorbents **2** and **4** at 25 °C (m/V = 100 mg dm^{-3}, $C_{As(V)}$ = 0.19 mg dm^{-3}, pH = 3.8).

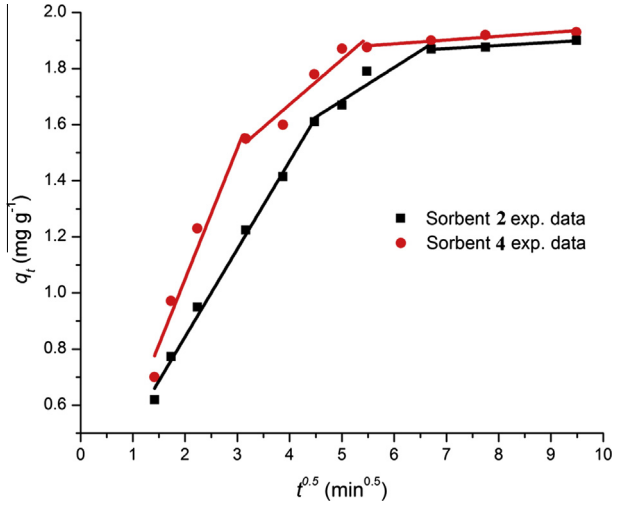

Fig. 6. Intraparticle diffusion plot for arsenate adsorption onto sorbents **2** and **4** at 25 °C (m/V = 100 mg dm^{-3}, $C_{As(V)}$ = 0.19 mg dm^{-3}, pH = 3.8).

treatment adsorbent particle destruction was not a notable process.

3.11. Mechanism of arsenate adsorption

Mechanism of arsenate adsorption onto goethite was commonly studied by extended X-ray adsorption fine structure (EXAFS) and FTIR spectroscopy, while study on influence of solution ionic strength and shift of isoelectric point could be used an additional indication on the adsorption mechanism. It has been shown that adsorption properties of goethite are mainly due to the existence of OH_2^+, OH, and O^- functional groups which under appropriate solution pH develop surface charges, *i.e.* protonation/deprotonation reactions, which are adsorbing sites for arsenate ions. At neutral and acidic pH (less than 8), OH_2^+ and OH forms of goethite surface are dominant and responsible for the selective binding of molecular and ionic forms of arsenic species [62]. Good accordance of the pH_{fin}/pH_{in} change results (Fig. S13) with proposed mechanism is obtained. Using EXAFS method, based on oxyanion-Fe distance, Fendorf et al. [47] defined existence of three different arsenate surface complexes on goethite: a monodentate, a bidentate-binuclear and a bidentate-mononuclear where the prevalent of complex depends on coverage degree. In the following research [63], two-step adsorption mechanism has been proposed. The first fast step involved initial ligand exchange forming a monodentate complex, while the next slow step represents a second ligand exchange resulting in the formation of an inner-sphere bidentate complex, *e.g.*, monodentate vs. bidentate, mononuclear vs. binuclear. The same type of complex was found by using macroscopic (point of zero charge shifts and ionic strength effect) and microscopic (Raman and FTIR spectroscopic) method of arsenate adsorption on amorphous iron oxide [51]. Intensification of adsorption with increasing of solution ionic strength is explained in the work of McBride [64] in the manner that adsorbed anions by inner-sphere association either show little sensitivity to ionic strength or respond with greater adsorption at higher ionic strength of solution. Similar situation could be explained by promoted arsenate adsorption in alkaline pH range. The increased adsorption of As(V), forming an inner-sphere complexes, cause negative charge build up, *i.e.* increases the net negative charge at adsorbent surface. If ionic strength of solution is high, increased concentration of counter cations are available to compensate the surface negative charge generated by specific adsorption of As(V). This phenomena favoured As(V) adsorption in presence of cations or increased ionic strength of solution (Fig. S10). Additionally, shift of isoelectric point of goethite with specifically adsorbed anions to lower value (Table S3) and results of FTIR analysis (Fig. S4) confirmed formation of inner-sphere surface complexes of As(V) anions and the surface of goethite and α-MnO_2.

Table 6
Calculated Gibbs free energy, enthalpy and entropy for arsenate adsorption.

Sorbent	$\Delta G°$ (kJ mol^{-1})			ΔH_o (kJ mol^{-1})	$\Delta S°$ (J mol^{-1} K^{-1})
	298 K	308 K	318 K		
2	−48.64	−43.05	−43.09	−132.25	283.41
4	−47.61	−43.71	−42.51	−124.05	257.79

The presented work was focused on development of composite adsorbent materials based on solvothermally synthesized calcite with improved morphological properties, and study of their adsorption characteristics. Results presented herein showed significant improvement of adsorbent properties of composite materials based on synthetic calcite and subsequent goethite, α-MnO_2 and goethite/α-MnO_2 precipitation vs. some reported adsorbents for arsenate removal (Table S6). The optimal methods for goethite and goethite/α-MnO_2 loading on calcite were developed, implying that morphology of synthesized calcite and optimal method of metal precipitation are the main factors influencing adsorbent properties. Modeling of experimental adsorption data, using

MINTEQ program, helps in understanding relation between different solution parameters and adsorption processes.

4. Conclusion

In conclusion, arsenate adsorption was effectively accomplished by a series of composite adsorbents based on solvothermal synthesis of highly porous calcite and subsequent precipitation of goethite, α-MnO_2 and goethite/α-MnO_2. Application of ultrasound had a large impact on improving adsorption performance whereas the modification gave the best results for optimal goethite (sorbent **2**) and hybrid system goethite/α-MnO_2 loading (sorbent **4**). The adsorption pattern of arsenate removal for sorbents **2** and **4** fitted well to Khan and Jovanovic model and the adsorption capacities obtained from Langmuir isotherms were 20.92 and 41.81 mg g^{-1} at 25 °C, respectively. The pseudo-second-order equation and intra-particle diffusion model well described the kinetic data and adsorption processes indicating that both arsenic and surface groups contribute to the overall adsorption mechanism. The best adsorption capability of sorbent **4** was discussed to be consequence of adsorbent highest specific surface area, mesopore volume and diameter, as well as synergetic effect of hybrid nature of goethite/α-MnO_2 composite. Influence of coexisting ions, in concentrations usually found in natural waters, showed negligible impact on arsenate removal at pH 4, except phosphate which caused the greatest arsenate percentage adsorption decrease. Results of theoretical modeling, obtained by the use of DLM model incorporated in MINTEQ, was in a good agreement with experimental data. The results of thermodynamic study, negative values of Gibbs free energy changes, positive standard entropy changes and negative values of enthalpy, indicate spontaneity of sorption processes which are more favorable at lower temperature.

Acknowledgements

The authors acknowledge financial support from Ministry of Education, Science and Technological development of Serbia, Projects No. III43009 and 172007.

Appendix A. Supplementary data

Supplementary data associated with this article can be found, in the online version, at http://dx.doi.org/10.1016/j.ultsonch.2013.10.006.

References

[1] P. Ravenscroft, H. Brammer, K. Richards, Arsenic Pollution: A Global Synthesis, John Wiley & Sons, United Kingdom, 2009.
[2] P.L. Smedley, D.G. Kinniburgh, A review of the source, behaviour and distribution of arsenic in natural waters, Appl. Geochem. 17 (2002) 517–568.
[3] C.O. Abernathy, M. Beringer, R.L. Calderon, T. McMahon, E. Winchester, An update on some arsenic programs at the US EPA, in: W.R. Chappell, C.O. Abernathy, R.L. Calderon, P.J. Thomas (Eds.), Proceedings of the Fifth International Conference on Arsenic Exposure and Health Effects, San Diego, California, 2002.
[4] R.M. Azizur, H. Hasegawa, Arsenic in freshwater systems. Influence of eutrophication on occurrence, distribution, speciation, and bioaccumulation, Appl. Geochem. 27 (2012) 304–314.
[5] World Health Organization (WHO), Guidelines for drinking water quality, Third Edition incorporating first and second addenda, vol. 1, Recommendations, Geneva, Switzerland, WHO, 2008, 491–492.
[6] M.S. Sinicropi, D. Amantea, A. Caruso, C. Saturnino, Chemical and biological properties of toxic metals and use of chelating agents for the pharmacological treatment of metal poisoning, Arch. Toxicol. 84 (2010) 501–520.
[7] D.N. Guha Mazumder, Chronic arsenic toxicity & human health, Indian, J. Med. Res. 128 (2008) 436–447.
[8] T.S.Y. Choong, T.G. Chuah, Y. Robiah, F.L. Gregory Koay, I. Azni, Arsenic toxicity, health hazards and removal techniques from water: an overview, Desalination 217 (2007) 139–166.
[9] M. Hua, S. Zhang, B. Pan, W. Zhang, L. Lv, Q. Zhang, Heavy metal removal from water/by nanosized metal oxides: A review, J. Hazard. Mater. 211–212 (2012) 317–331.
[10] Z. Veličković, G.D. Vuković, A.D. Marinković, M.-S. Moldovan, A.A. Perić-Grujić, P.S. Uskoković, M.Đ. Ristić, Adsorption of arsenate on iron(III) oxide coated ethylenediamine functionalized multiwall carbon nanotubes, Chem. Eng. J. 181–182 (2012) 174–181.
[11] L.H.E. Winkel, B. Casentini, F. Bardelli, A. Voegelin, N.P. Nikolaidis, L. Charlet, Speciation of arsenic in Greek travertines: co-precipitation of arsenate with calcite, Geochim. Cosmochim. Acta 106 (2013) 99–110.
[12] D.E. Giles, M. Mohapatra, T.B. Issa, S. Anand, P. Singh, Iron and aluminium based adsorption strategies for removing arsenic from water, J. Environ. Manage. 92 (2011) 3011–3022.
[13] D.N. Thanh, M. Singh, P. Uldrich, F. Štěpánek, N. Stradanová, As(V) removal from aqueous media using α-MnO_2 nanorods-impregnated laterite composite adsorbents, Mater. Res. Bull. 47 (2012) 42–50.
[14] G.-S. Zhang, J.-H. Qu, H.-J. Liu, R.-P. Liu, G.-T. Li, Removal mechanism of As(III) by a novel Fe-Mn binary oxide adsorbent: oxidation and sorption, Environ. Sci. Technol. 41 (2007) 4613–4619.
[15] G. Zhang, H. Liu, R. Liu, J. Qu, Adsorption behavior and mechanism of arsenate at Fe–Mn binary oxide/water interface, J. Hazard. Mater. 168 (2009) 820–825.
[16] M.H. Entezari, T. Rohani Bastami, Influence of ultrasound on cadmium ion removal by sorption process, Ultrason. Sonochem. 15 (2008) 428–432.
[17] J.-B. Ji, X.-H. Lu, Z.-C. Xu, Effect of ultrasound on adsorption of Geniposide on polymeric resin, Ultrason. Sonochem. 13 (2006) 463–470.
[18] L. Nouri, O. Hamdaoui, Ultrasonication-assisted sorption of cadmium from aqueous phase by wheat bran, J. Phys. Chem. A 111 (2007) 8456–8463.
[19] L. Paniwnyk, E. Beaufoy, J.P. Lorimer, T.J. Mason, The extraction of rutin from flower buds of Sophora japonica, Ultrason. Sonochem. 8 (2001) 299–301.
[20] M. Vinatoru, M. Toma, O. Radu, P.I. Filip, D. Lazurca, T.J. Mason, The use of ultrasound for the extraction of bioactive principles from plant materials, Ultrason. Sonochem. 4 (1997) 135–139.
[21] M. Breitbach, D. Bathen, Influence of ultrasound on adsorption processes, Ultrason. Sonochem. 8 (2001) 277–283.
[22] O. Hamdaoui, E. Naffrechoux, Adsorption kinetics of 4-chlorophenol onto granular activated carbon in the presence of high frequency ultrasound, Ultrason. Sonochem. 16 (2009) 15–22.
[23] O. Hamdaoui, E. Naffrechoux, L. Tifouti, C. Pétrier, Effects of ultrasound on adsorption–desorption of p-chlorophenol on granular activated carbon, Ultrason. Sonochem. 10 (2003) 109–114.
[24] O. Hamdaoui, R. Djeribi, E. Naffrechoux, Desorption of metal ions from activated carbon in the presence of ultrasound, Ind. Eng. Chem. Res. 44 (2005) 4737–4744.
[25] O. Hamdaoui, E. Naffrechoux, J. Suptil, C. Fachinger, Ultrasonic desorption of *p*-chlorophenol from granular activated carbon, Chem. Eng. J. 106 (2005) 153–161.
[26] O. Hamdaoui, E. Naffrechoux, An investigation of the mechanisms of ultrasonically enhanced desorption, AIChE J. 53 (2007) 363–373.
[27] V. Suchkova, E.L. Carstensen, C.W. Francis, Ultrasound enhancement of fibrinolysis at frequencies of 27 to 100 kHz, Ultrasound Med. Biol. 28 (2002) 377–382.
[28] S.L. Poliachik, W.L. Chandler, P.D. Mourad, M.R. Bailey, B. Susannah, R.O. Cleveland, P. Kaczkowski, G. Keilman, T. Porter, L.A. Crum, Effect of highintensity focused ultrasound on whole blood with and without microbubble contrast agent, Ultrasound Med. Biol. 25 (1999) 991–998.
[29] A.E. Worthington, J. Thompson, A.M. Rauth, J.W. Hunt, Mechanism of ultrasound enhanced porphyrin cytotoxicity. Part I: a search for free radical effects, Ultrasound Med. Biol. 23 (1997) 1095–1105.
[30] D.V. Sakharov, R.T. Hekkenberg, D.C. Rijken, Acceleration of fibrinolysis by high-frequency ultrasound: the contribution of acoustic streaming and temperature rise, Thromb. Res. 100 (2000) 333–340.
[31] H.M. Santos, C. Lodeiro, J.-L. Capelo-Martínez, Ultrasound in Chemistry: Analytical Applications, WILEY-VCH Verlag GmbH & Co. KGaA, Weinheim, 2009.
[32] T.J. Mason, Practical Sonochemistry: User's Guide to Applications in Chemistry and Chemical Engineering, Ellis Horwood, Chichester, 1991.
[33] L.H. Thompson, L.K. Doraiswamy, Sonochemistry: science and engineering, Ind. Eng. Chem. Res. 38 (1999) 1215–1249.
[34] J.P. Gustafsson, Visual MINTEQ 3.0, beta, http://www.lwr.kth.se/English/OurSoftware/-vminteq/index.htm, Stockholm, Sweden, 2011.
[35] Z. Zhao, L. Zhang, H. Dai, Y. Dub, X. Meng, R. Zhang, Y. Liu, J. Deng, Surfactant-assisted solvo- or hydrothermal fabrication and characterization of high-surface-area porous calcium carbonate with multiple morphologies, Microporous Mesoporous Mater. 138 (2011) 191–199.
[36] U. Schwertmann, R.M. Cornell, Iron Oxides in the Laboratory, Preparation and Characterization, second ed., WILEY-VCH Verlag GmbH, 2000.
[37] E. Erdem, N. Karapinar, R. Donat, The removal of heavy metal cations by natural zeolites, J. Colloid Interface Sci. 280 (2004) 309–314.
[38] G.D. Vuković, A.D. Marinković, S.D. Škapin, M.Đ. Ristić, R. Aleksić, A.A. Perić-Grujić, P.S. Uskoković, Removal of lead from water by amino modified multi-walled carbon nanotubes, Chem. Eng. J. 173 (3) (2011) 855–865.
[39] K.Y. Foo, B.H. Hameed, Insights into the modeling of adsorption isotherm systems, Chem. Eng. J. 156 (2010) 2–10.
[40] W.D. Schecher, D.C. McAvoy, MINEQL+: User's Manual, Environmental Research Software, Edgewater, Hallowell, Maine, USA, 2001.

[41] D.A. Dzombak, F.M.M. Morel, Surface Complexation Modeling: Hydrous Ferric Oxide, John Wiley & Sons Inc., New York, 1990.
[42] J.G. Hering, P.-Y. Chen, J.A. Wilkie, M. Elimelech, S. Liang, Arsenic removal by ferric chloride, J. Am. Water Works Assn. 88 (1996) 155–167.
[43] P.J. Pretorius, P.W. Linder, Determination of diffuse double layer protonation constants for hydrous ferric oxide (HFO): supporting evidence for the Dzombak and Morel compilation, Chem. Speciation Bioavailability 10 (1998) 115–119.
[44] S.D. Cifrulak, High pressure mid-infrared studies of calcium carbonate, Am. Mineral. 55 (1970) 815–824.
[45] B. Yang, Q. Gong, L. Zhao, H. Sun, N. Ren, J. Qin, J. Xu, H. Yang, Preconcentration and determination of lead and cadmium in water samples with a MnO_2 coated carbon nanotubes by using ETAAS, Desalination 278 (2011) 65–69.
[46] S. Myneni, S. Traina, G. Waychunas, T. Logan, Experimental and theoretical vibrational spectroscopic evaluation of arsenate coordination in aqueous solutions, solids, and an mineral-water interfaces, Geochim. Cosmochim. Acta 62 (1998) 3285–3300.
[47] S. Fendorf, M.J. Eick, P. Grossl, D.L. Sparks, Arsenate and chromate retention mechanisms on goethite. 1. Surface structure, Environ. Sci. Technol. 31 (1997) 315–320.
[48] S. Goldberg, Adsorption Models Incorporated into Chemical Equilibrium, Chemical Equilibrium and Reaction Models, SSSA Special Publication 42, Models Soil Science Society of America, American Society of Agronomy, USA, 1995.
[49] A. Maiti, J.K. Basu, S. De, Experimental and kinetic modeling of As(V) and As(III) adsorption on treated laterite using synthetic and contaminated groundwater: effects of phosphate, silicate and carbonate ions, Chem. Eng. J. 191 (2012) 1–12.
[50] M. Stachowicz, T. Hiemstra, W.H. van Riemsdijk, Multi-competitive interaction of As(III) and As(V) oxyanions with Ca^{2+}, Mg^{2+}, PO_4^{3-}, and CO_3^{2-} ions on goethite, J. Colloid Interface Sci. 320 (2008) 400–414.
[51] S. Goldberg, C.T. Johnston, Mechanisms of arsenic adsorption on amorphous oxides evaluated using macroscopic measurements, vibrational spectroscopy, and surface complexation modeling, J. Colloid Interface Sci. 234 (2001) 204–216.
[52] S. Goldberg, Competitive adsorption of arsenate and arsenite on oxides and clay minerals, Soil Sci. Soc. Am. J. 66 (2002) 413–442.
[53] I. Quiñones, G. Guiochon, Derivation and application of a jovanovic–freundlich isotherm model for single-component adsorption on heterogeneous surfaces, J. Colloid Interface Sci. 183 (1996) 57–67.
[54] I. Langmuir, The constitution and fundamental properties of solids and liquids, J. Am. Chem. Soc. 38 (1916) 2221–2295.
[55] M.C. Ncibi, Applicability of some statistical tools to predict optimum adsorption isotherm after linear and non-linear regression analysis, J. Hazard. Mater. 153 (2008) 207–212.
[56] H. Qiu, L. Lv, B. Pan, Q. Zhang, W. Zhang, Q. Zhang, Critical review in adsorption kinetic models, Univ. Sci. A 10 (5) (2009) 716–724.
[57] W.J. Weber, J.C. Morris, Kinetics of adsorption on carbon from solution, J. Sanit. Eng. 89 (1963) 31–59.
[58] M. D'Arcy, D. Weiss, M. Bluck, R. Vilar, Adsorption kinetics, capacity and mechanism of arsenate and phosphate on a bifunctional TiO_2-Fe_2O_3 bi-composite, J. Colloid Interface Sci. 364 (2011) 205–212.
[59] C. Luo, R. Wei, D. Guo, S. Zhang, S. Yan, Adsorption behavior of MnO_2 functionalized multi-walled carbon nanotubes for the removal of cadmium from aqueous solutions, Chem. Eng. J. 225 (2013) 406–415.
[60] C.-C. Liu, M. Kuang-Wang, Y.-S. Li, Removal of nickel from aqueous solution using wine processing waste sludge, Ind. Eng. Chem. Res. 44 (2005) 1438–1445.
[61] D. Mohan, C.U. Pittman, Arsenic removal from water/wastewater using adsorbents-a critical review, J. Hazard. Mater. 142 (2007) 1–53.
[62] N. Ben Issa, V.N. Rajaković-Ognjanović, B.M. Jovanović, Lj V. Rajaković, Determination of inorganic arsenic species in natural waters–benefits of separation and preconcentration on ion exchange and hybrid resins, Anal. Chim. Acta 673 (2010) 185–193.
[63] P.R. Grossl, M. Eick, D. Sparks, S. Goldberg, C.C. Ainsworth, Arsenate and chromate retention mechanisms on goethite. 2. Kinetic evaluation using a pressure-jump relaxation technique, Environ. Sci. Technol. 31 (1997) 321–326.
[64] M.B. McBride, A critique of diffuse double layer models applied to colloid and surface chemistry, Clay Miner. 45 (1997) 598–608.